BEILSTEIN ARCHIVES

This open access document is posted as a preprint in the Beilstein Archives at https://doi.org/10.3762/bxiv.2021.2.v1 and is considered to be an early communication for feedback before peer review. Before citing this document, please check if a final, peer-reviewed version has been published.

This document is not formatted, has not undergone copyediting or typesetting, and may contain errors, unsubstantiated scientific claims or preliminary data.

Preprint Title Correlative analysis of embedded silicon interfaces passivation by “Kelvin probe force microscopy” and “corona oxide characterization of semiconductor”

Authors Valentin Aubriet, Kristell Courouble, Mickael Gros-Jean and Lukasz Borowik

Publication Date 13 Jan. 2021

Article Type Full Research Paper

ORCID® iDs Mickael Gros-Jean - https://orcid.org/0000-0002-7700-032X; Lukasz Borowik - https://orcid.org/0000-0002-7472-1105

License and Terms: This document is copyright 2021 the Author(s); licensee Beilstein-Institut.

This is an open access work under the terms of the Creative Commons Attribution License (https://creativecommons.org/licenses/by/4.0). Please note that the reuse, redistribution and reproduction in particular requires that the author(s) and source are credited and that individual graphics may be subject to special legal provisions. The license is subject to the Beilstein Archives terms and conditions: https://www.beilstein-archives.org/xiv/terms.
The definitive version of this work can be found at https://doi.org/10.3762/bxiv.2021.2.v1

Correlative analysis of embedded silicon interfaces passivation by “Kelvin probe force microscopy” and “corona oxide characterization of semiconductor”

Valentin Aubriet[1,2], Kristell Courouble[2], Mickael Gros-Jean[2], and Łukasz Borowik[1]*

[1] Univ. Grenoble Alpes, CEA, Leti, F-38000 Grenoble, France

[2] STMicroelectronics, 850 rue Jean Monnet, 38926 Crolles Cedex France

*corresponding author : Lukasz.Borowik@cea.fr

ABSTRACT: We report a correlative analysis between corona oxide characterization of semiconductor (COCOS) and Kelvin probe force microscopy (KPFM) for the study of embedded silicon-oxide interfaces in the field of chemical and field-effect passivation. Analyzed parameters by these measurements are linked to different factors and specifically to defects density of embedded silicon-dielectric interfaces, surface band bending or the distribution of charges in the nearest surface volume.

Furthermore, this COCOS-KPFM correlative analysis turns out to be a useful method to access to chemical and field-effect passivation. We confirm that it is possible to differentiate the influence of local band bending on sample passivation (i.e. field effect passivation) from the effects due to the local recombination rates (i.e. chemical passivation).

The measurements were carried on five different passivation layers, precisely, 10.5 nm-thick SiO_2, 50 nm-thick SiN, 7nm-thick Al_2O_3, 7 nm-thick HfO_2 and double layer of 7 nm-thick Al_2O_3 below 53 nm-thick Ta_2O_5. This correlative analysis indicates that HfO_2 present to be the best chemical passivation and SiN is the worst case in term of field effect passivation for p-type silicon. Additionally, we confirm that Ta_2O_5 layer on top of Al_2O_3 increase the defects density.

KEYWORDS: silicon-dielectric interface, band bending, defects density, recombination rate, surface passivation

INTRODUCTION

Characterization of interfaces is essential for several types of devices like solar cells, photodetectors or LED devices. In the case of photodetectors, defects present at the interfaces impact the dark current which decrease the detector quality by producing false signal [1]. For solar cells, defects at the interfaces play an important role by limiting the amount of charges collected at the electrodes and thus degrading the solar cell efficiency [2]. In the case of LED, all non-radiatives defects must be as well reduced for the best device operation [3].

To overcome the issues related to defects, surface or interface passivation becomes mandatory. Previously, passivation has been studied in various materials [4–7] by means of two mechanisms, chemical passivation (decrease the density of defect) [8,9] and field effect passivation (introducing fixed positive or negative charges within a passivation layer) [10,11]. Depending on the device, the field effect passivation does not have the same significance. For example, in the case of solar cells or LEDs, the field effect passivation corresponds to the reduction of the density of one type of charge carrier in order to reduce carrier recombination process. For the photodetectors, the field

effect passivation aims to put the interface under a charge accumulation in order to neutralize defects responsible of dark current (through thermionic generation) [12]. In both cases, carrier generation and recombination are described by Shockley-Read-Hall theory and are highly dependent on defect density and defect energy position. For instance, the generation and recombination rates are the highest for mid-gap defects [12,13].

Over the years several methods have been implemented to characterize the silicon surface embedded under different types of passivation layers[14]. Among them, capacitance-voltage (C-V) is widely used for determining the chemical and field effect passivation. Specifically, C-V methods such as the Castagné-Vapaille method [15], the Terman method [16], the Berglund integral method [17] or the conductance method [18] has been employed. However, these methods require special sample preparation and a metal-oxide-semiconductor structure, which could lead to modification of the interface under investigation. In the frame of contactless method the corona oxide characterization of semiconductor (COCOS) appears to be an alternative to the C-V method for determining the chemical and field effect passivation properties [19].

Besides, Kelvin probe force microscopy (KPFM) is one of the most sensitive methods to probe surface potential related to work function (with sensitivity <5meV) [20]. Moreover, KPFM under illumination is a well-established method to measure surface photovoltage (SPV) and charge carrier lifetime over organic and inorganic materials [21][22][23]. In addition, previous study reports that charge carrier lifetime measured by KPFM through SPV can be sensitive to defects even when embedded in silicon dioxide [24]. However, until now the use of KPFM under illumination to study passivation of buried interface has not been reported.

In this paper, we will present the combined analysis by COCOS and KPFM under illumination to analyze the properties of embedded interfaces, as such measurement is still lacking and can be

complementary to C-V measurements. In the case of KPFM, besides of the capability to measure the simple SPV, the particularity of the setup used here is the capability to analysis this parameter as a function of different illumination wavelengths to perform in-depth dependent measurements. Such extracted SPV from KPFM measurements will be compared to total fixed charge (Qtot), density of defects (DiT) and barrier potential (V_{SB}) all probed by COCOS.

RESULTS AND DISCUSSION

In this work, we use non-contact atomic force microscopy (nc-AFM) (VT-AFM from ScientaOmicron interfaced with a Nanonis controller from SPECS Zürich) operating under ultra-high vacuum conditions (<10^{-10} Torr). We use here a metal-plated conductive tip (EFM PPP from Nanosensors) with a resonant frequency f_0=67 kHz. f_0 is mechanically excited to control the tip–surface distance by nc-AFM with a frequency shift set point equal to -20Hz. Specifically for the KPFM mode purposes, we use an additional lock-in amplifier (HF2LI from Zurich Instruments), where KPFM measurements were carried out in a single pass mode using heterodyne amplitude modulation KPFM (h-KPFM) [25][26][27]. In h-KPFM a bias voltage V_{ac} is applied at f_1-f_0 (f_0 and f_1 being the fundamental resonant frequency and its first harmonic respectively) which generate an electrostatic force at f_1 if the cantilever V_{dc} bias does not match the contact potential difference (CPD). To measure CPD, feedback loop is introduced to nullify the cantilever oscillation amplitude at f_1. It must be pointed out that the potential sensitivity is enhanced with increasing quality factor, making h-KPFM under UHV well suited for surface potential measurement [25]. For SPV measurements we use external fiber-coupled laser (PhoxXplus module from OmicronLaserage GmBH) at 405nm, 458nm, 515nm and 638nm in order to perform in depth measurements. The penetration depths for silicon substrate were measured by ellipsometry and are respectively: 97 nm, 433 nm, 1 µm, 3 µm for four used laser wavelengths.

The sample illumination is done through a viewport of the UHV chamber. Additionally, we measure the photon flux with a power meter (standard photodiode power sensor from Thorlabs) to know the photon flux in the function of laser power. Furthermore, we set the calibrated laser power to obtain a constant photon flux for each used here laser wavelength.

Under illumination, the absorption of a photon with an energy higher than the band-gap induces the generation of electrons-holes pairs. Here trap-to-band absorption is neglected since the probability of this process is low (i.e. photon energy higher than the silicon band gap), thus, we consider only super band-gap absorption [28]. After the generation process, electrons-holes pairs recombine with a time scale defined by the sample electronic properties (i.e. density of defects, energy of defect, capture cross-section, carrier density) [29]. SPV is the difference between CPD measured under sample illumination and measured when sample is in dark conditions as represented on Figure 2a. SPV is a surface quantity based on the reorganization of positive and negative charges (i.e. separation of electron-holes pairs) in the sample volume, when sample is under illumination. This charge reorganization and so the origin of SPV can be induced by surface band bending. Accordingly, one type of carrier diffuses toward the surface causing a partial band flattening while the other type diffuses toward the bulk. At high photon flux, the band may be completely flattened. We illustrate this process on Figure 1 with two different laser wavelengths excitations to show the influence of photon penetration depth on measured SPV. It is important to mention that SPV is not only highly sensitive to the surface, whereas this parameter can be also influenced by sample bulk properties due to the generation of carrier in the bulk [30] .

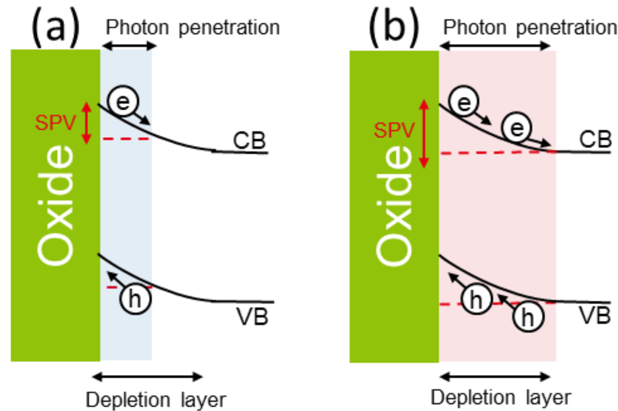

Figure 1. Schematic band diagram of the surface space charge region under accumulation of a p-type semiconductor for two different wavelengths. On both cases, under illumination the photo-generated electrons (holes) diffuse toward the bulk (or surface). In all diagrams, solid and dashed lines indicate band position under dark and illumination. SPV maximum amplitude is represented in red. CB and VB refer to conduction band and valence band respectively. (a) The photon penetration depth is shorter than the space charge region (b) The photon penetration depth is greater than the space charge region.

Specifically in our experimental protocol we kept the same photon fluxes between the different lasers wavelengths. Undoubtedly, due to different reflectivity coefficients over the different passivation layers, the absorbed photon flux cannot be set to ultimate constant values over the sample set. This effect will be commented later in this article.

SPV parameter measured by KPFM can be compared to COCOS measurement which is rather standard technique to characterize dielectrics for microelectronic technologies [19]. In this work the measurements are performed on 300 mm whole wafers using a FAaSTTM 230 from Semiconductor Diagnostics Incorporation. COCOS method is based on a sequential corona charge

(Q_c) deposition followed by the measurement of CPD in dark and under strong illumination (i.e to obtain flat band condition - V_{FB}), similarly to SPV measurement by KPFM. However, it must be noted that measurements are carried out with a macroscopic Kelvin probe. Corona charges are used to sweep interface from depletion to week accumulation. The difference between CPD under illumination and dark condition leads to the potential barrier (V_{SB}) as a function of deposited corona charges. The corona charges needed to obtain V_{SB}=0 represent the total amount of fixed charges (algebraic sum – including interface with silicon) (Q_{tot}). Thus, it corresponds to the total amount of corona charges needed to switch V_{SB} from its initial value ($V_{SB\ init}$) to 0 (V_{FB}). $V_{SB\ init}$ refers to the potential barrier before charge deposition. Figure 2b shows CPD probed by COCOS under dark and illumination condition with respect to Q_c. The density interface trap (DiT) is calculated from the ratio $\Delta Q_{it}/\Delta V_{SB}$, where ΔQ_{it} is the charge trapped at the interface due to a quanta of corona charges and ΔV_{SB} is the change in barrier potential due to a quanta of corona charges. ΔQ_{it} is calculated from the difference between space charge region charges and corona charges.

DiT, Q_{tot} and V_{SB} presented in this report correspond to the averaged value of nine measurements per sample. The standard deviation will be presented to give information about the dispersion of the parameters measured.

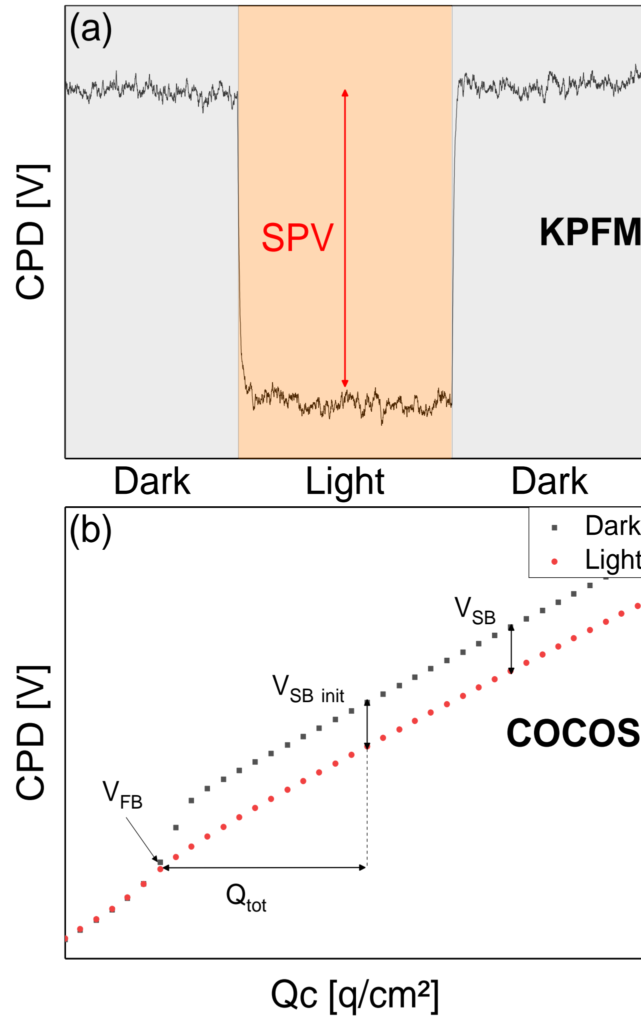

Figure 2. (a) h-KPFM measurements under dark condition and illumination conditions. After illumination, CPD comes back to its initial value. SPV amplitude is represented by the red arrow. (b) CPD with respect to the corona charge deposition probed by COCOS.

To study the passivation of buried interface we analyzed silicon substrates with five different passivation layers. Precisely, 10.5 nm-thick SiO_2, 50 nm-thick SiN, 7 nm-thick Al_2O_3, 7 nm-thick HfO_2 and double layer of 7 nm-thick Al_2O_3 below 53 nm-thick Ta_2O_5 were used as passivation layers on boron doped (100) oriented 300 mm CZ silicon wafer (N_D=1E15 at/cm^3). Samples were prepared by various processes, specifically, SiO_2 were prepared with Rapid Thermal Oxidation (RTO), SiN with Plasma Enhanced Chemical Vapor Deposition (PECVD), Al_2O_3 and HfO_2 were

grown using Atomic Layer Deposition (ALD) using H_2O as reactant and respectively $Al(CH_3)_3$ and $HfCl_4$ as precursor. Ta_2O_5 layers were deposited by Plasma Enhanced ALD (PEALD) using (Tert-Butylimido Tris(DiEthylamino) Tantalum) as Ta precursor and O_2 plasma. Subsequently, all samples were annealed at 400°C during 120 min under nitrogen.

On Figure 4. we present the experimental results from COCOS and KPFM measurements for all five passivation layers. Firstly, on Figure 4a and Figure 4b we present respectively Q_{tot} and V_{SB} measurements by COCOS. The amplitudes of these two quantities are self-dependent since the band-bending is caused by the presence of defects and fixed charges present at the silicon surface and within the passivation layer. In other words, in order to respect the charge neutrality, the bands are bent in the vicinity of the surface. Negative (or positive) charges contained in the passivation stack involve upward (or downward) band bending. The Q_{tot} and V_{SB} quantities can be compared with KPFM measurements on Figure 4d and Figure 4e where we present respectively the evolution of the normalized SPV with respect to the laser power (i.e. photon flux) at wavelength of 638 nm and the maximum SPV amplitude (i.e. when saturation of the SPV is obtained) for 405 nm, 457 nm, 515 nm and 638 nm wavelengths. In the case of KPFM under illumination, photo-generated charges diffuse toward the surface accordingly to the direction of the band-bending. Consequently, the positive (or negative) SPV probed with KPFM is consistent with a downward (or upward) band bending probed with COCOS since under illumination, it implies diffusion of holes toward the surface for HfO_2, Al_2O_3 and Al_2O_3/Ta_2O_5 and electrons toward the surface for SiN and SiO_2. We want to emphasis that this phenomenon of charge transfers which is at the origin of the SPV is reversible when switching the light on and off and observing that SPV values are reproducible under illumination and the surface potential always goes back to the initial value

under dark conditions. Due to such reversibility, we can assume the negligible contribution of charge trapping phenomenon in the case of these five passivation layers.

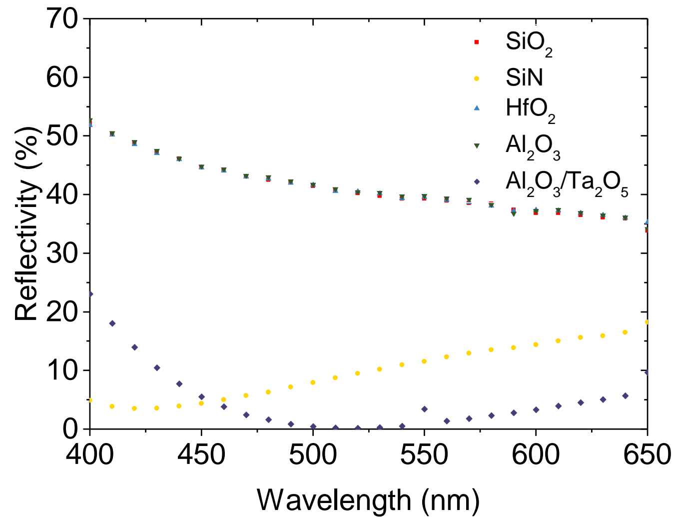

Figure 3. Reflectivity of SiO_2, SiN, HfO_2, Al_2O_3 and Al_2O_3/Ta_2O_5 on p-type Si (100) in the 400-650 nm range

for different laser power and is dependent of the passivation layer. To explain this phenomenon, we must address the possible effects of different reflectivity coefficient over the visible range. Since the number of generated electron-hole pairs is related to the number of absorbed photons under illumination, SPV can be potentially influenced by change of reflectivity in the function of wavelength presented on Figure 3. However, the variation of the SPV amplitude seems not to be correlated to the optical properties since Al_2O_3, HfO_2 and SiO_2 present the same reflectivity coefficient over the visible range. Moreover, Al_2O_3 and Al_2O_3/Ta_2O_5 samples present significantly different reflectivity coefficient. Accordingly, we would expect a higher SPV amplitude for Al_2O_3/Ta_2O_5 since a higher photon flux reaches the silicon surface than for Al_2O_3. Nevertheless, experimental measurements show the opposite behavior with lower SPV for Al_2O_3/Ta_2O_5

comparing to Al_2O_3. Consequently, we consider that maximum SPV at flat band regime is rather not linked (or not considerably influenced) with different reflectivity coefficients.

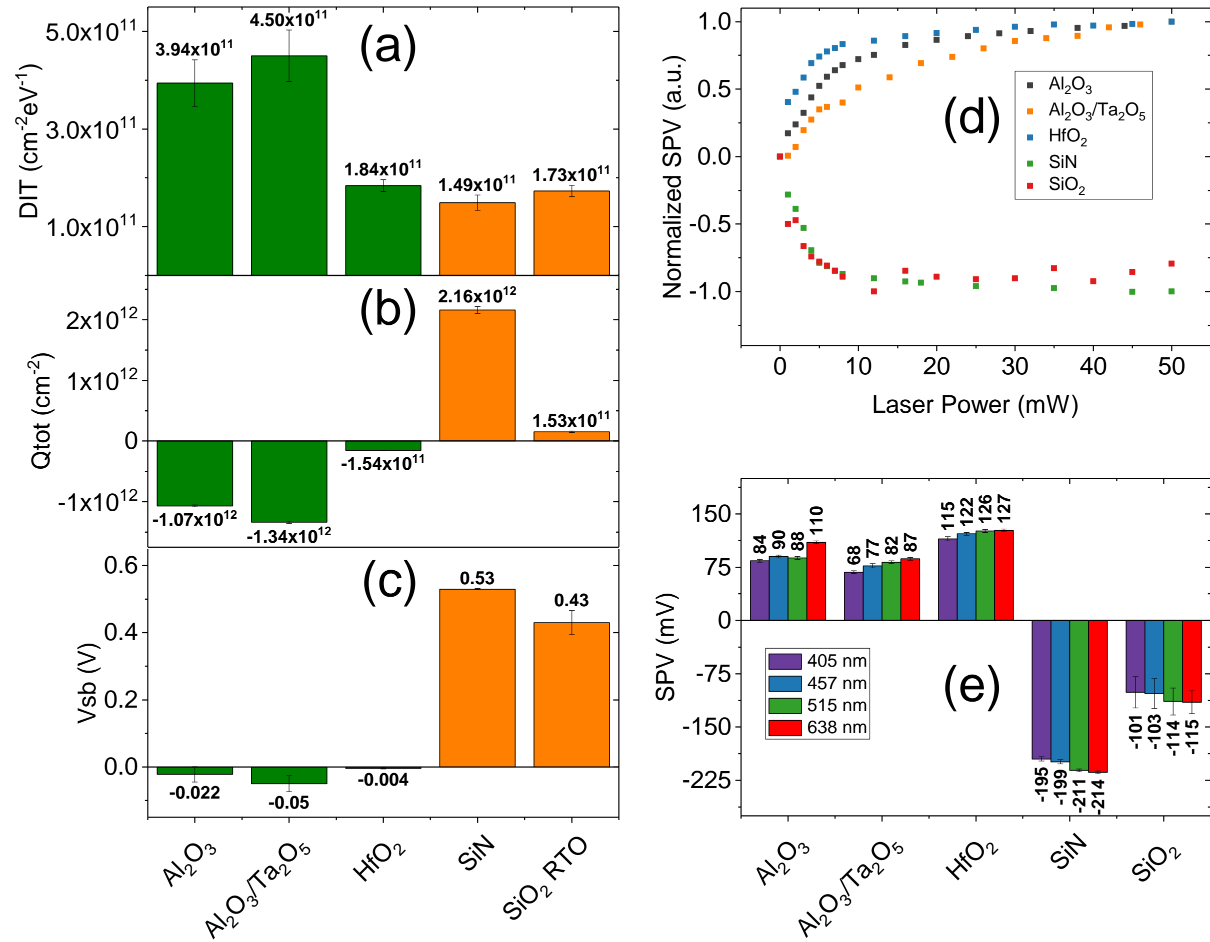

Figure 4. All diagrams aims to compare COCOS (a),(b),(c) with KPFM (d),(e). (a) Total amount of all dielectric charges (algebraic sum – including interface with silicon). (b) Barrier potential across the surface space charge region. (c) Density of defects at the interface between silicon and dielectric. (d) Evolution of the normalized SPV with respect to the laser power at 638nm. (e) SPV amplitude under flat band condition laser 405nm, 457nm, 515nm and 638nm.

Another parameter which can be considered to influence the SPV is the minimum DiT over silicon band gap. DiT values for the five passivation layers are presented on Figure 4c. We notice that SiN present the lowest and Al_2O_3/Ta_2O_5 the highest DiT of our five sample set. DiT correlates with SPV since a high DiT requires stronger illumination power to reach the saturation regime and the maximum SPV amplitudes appears to be lower when the DiT increases. For the more accurate analysis of SPV amplitude the simple comparison with DiT is not sufficient and all three parameters Q_{tot}, V_{SB} and DiT must be taken to account. We notice that SiN and SiO_2 present nearly the same DiT and V_{SB}, and even if we consequently observe similar variation of the SPV amplitude with respect to the laser power, SPV maximum amplitude for SiN appears to be two-times higher than for SiO_2. This observation seems to be correlated to the total amount of fixed charges which is one decade higher for SiN than for SiO_2. The last remark suggests that in order to respect charge neutrality, the larger quantity of fixed charges contained within SiN induces a larger reorganization of the photo generated charges in silicon (i.e. increase of the SPV maximum amplitude). Additionally on Figure 4e we indicate an evolution of SPV amplitude according to the wavelength of the illumination source (i.e. four penetration depths). This effect might be due to the change of the penetration depth. In fact, the 405nm light source generates in-depth carriers in over 100 nm, in comparison to 3 µm with 638 nm light source. So here we expect the penetration depth to be a limiting factor to the SPV amplitude. As well, we expect the diminution of the penetration depth to increase the contribution of the Auger recombination process due the confinement of the carriers.

Thus, this correlative analysis shows that SPV signal can be very useful for the band bending sign (downward or upward) verification, as well as the analysis of the maximum value of SPV which corresponds to the quantity of charges necessary for flat bands regime. However, for more

accurate analysis of SPV the additional Q_{tot}, V_{SB} and DiT parameters from COCOS measurement should be taken to account to evaluate the impact of each of these parameters.

Furthermore, we point out that a previous study reports as well the relation between photovoltage, laser intensity and defects on silicon (7x7) surface [31]. From Figure 4d, we notice the logarithmic evolution of the SPV with respect to the laser power, and thus, we can fit the SPV evolution with the following equation: SPV = A*ln(1+BI) where A is proportional to the band bending and BI describes the ratio of carrier generation rate to the recombination rate [31]. Fitted parameters are presented on Figure 5a and Figure 5b respectively. We notice that when Q_{tot} (or V_{SB}) decreases the amplitude of the A parameter decreases as well. This dependence is particularly

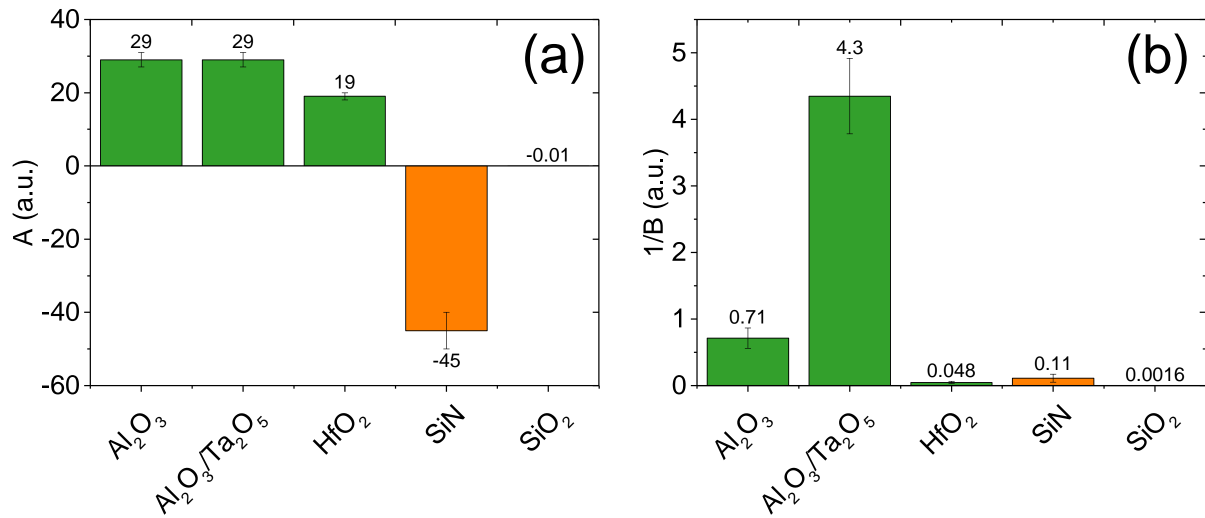

Figure 5. The SPV evolution with respect to the laser power can be fitted with the following model, SPV=A*ln(1+BI) [31]. (a) and (b) represent the evolution of A and 1/B over our sample set which depends on the local band bending and the recombination rate respectively.

pronounced on SiN and SiO_2 due the large density of fixed charges contained in SiN with strongly influence the local band bending. Additionally, we remark that the 1/B parameter variation can be attributed to the DiT variation. In fact, increase of the recombination rates (i.e. increase of 1/B) is

consistent with an increase of the DiT since defects present at the interface act as recombination center.

Concerning the contribution of this correlative analysis for silicon-oxide interfaces it comes out that local measurements through the KPFM tip and macroscopic measurements through the COCOS probe indicates both that HfO_2 present the best chemical passivation under the accumulation regimes (i.e. lowest DiT and recombination rate). On top of that we confirm by KPFM that the addition of the Ta_2O_5 layer on top of Al_2O_3 increases the recombination rate which is consistent with an increase of DiT. Such degradation appears to be consistent with the use of O_2 plasma for Ta_2O_5 deposition [32]. Finally, SiN shows to be clearly the worst case in term of field effect passivation for p-type silicon as shown by a positive potential barrier (i.e. accumulation regime) and so a negative SPV (i.e. diffusion of electrons toward the surface).

CONCLUSION

In this article we presented the correlative analysis by COCOS and KPFM showing to be a relevant and a straightforward method to study embedded silicon interface in the field of passivation. This analysis shows that SPV sign and amplitude is related to defects density, local band bending and to the distribution of fixed charges in the nearest surface volume. Additionally, by the KPFM analysis of the SPV as a function of laser power as well as the analysis of COCOS results, we confirm that it is possible to differentiate the effects due to local band bending (i.e. field effect passivation) from the effects due to the local recombination rates (i.e. chemical passivation) by KPFM.

This correlative analysis by COCOS and KPFM can be useful for other developments and especially can conduct correlative analysis of SPV images or can be helpful for charge carrier dynamical phenomenon analysis.

ACKNOWLEDGEMENTS

We want to thank Dr. Benjamin Grévin (CNRS, CEA, IRIG-SyMMES) for help on h-KPFM implementation. This work, done on the NanoCharacterisation PlatForm (PFNC), was supported by the "Recherches Technologiques de Base" Program of the French Ministry of Research.

REFERENCES

(1) Mcgrath, D.; Tobin, S.; Systems, B. A. E.; Goiffon, V.; Isae-supaero, P. M. **2018**, 1–8

(2) Bonilla, R. S.; Hoex, B.; Hamer, P.; Wilshaw, P. R. *Phys. Status Solidi Appl. Mater. Sci.* **2017**, *214* (7).

(3) Haller, C.; Carlin, J. F.; Jacopin, G.; Martin, D.; Butté, R.; Grandjean, N. *Appl. Phys. Lett.* **2017**, *111* (26).

(4) Seguini, G.; Cianci, E.; Wiemer, C.; Saynova, D.; Van Roosmalen, J. A. M.; Perego, M. *Appl. Phys. Lett.* **2013**, *102* (13).

(5) Wan, Y.; Bullock, J.; Hettick, M.; Xu, Z.; Yan, D.; Peng, J.; Javey, A.; Cuevas, A. *Appl. Phys. Lett.* **2018**, *112* (20), 1–5.

(6) Panigrahi, J.; Vandana; Singh, R.; Singh, P. K. *Sol. Energy Mater. Sol. Cells* **2018**.

(7) Krugel, G.; Sharma, A.; Wolke, W.; Rentsch, J.; Preu, R. *Phys. Status Solidi - Rapid Res. Lett.* **2013**.

(8) Dingemans, G.; Kessels, W. M. M. *J. Vac. Sci. Technol. A Vacuum, Surfaces, Film.* **2012**.

(9) Bonilla, R. S.; Hoex, B.; Hamer, P.; Wilshaw, P. R. *Phys. Status Solidi Appl. Mater. Sci.* **2017**.

(10) Glunz, S. W.; Biro, D.; Rein, S.; Warta, W. *J. Appl. Phys.* **1999**, *86* (1), 683–691.

(11) Aber;e, A. G.; Glunz, S.; Warta, W. *Sol. Energy Mater. Sol. Cells* **1993**, *29* (2), 175–182.

(12) Carrere, J. P.; Place, S.; Oddou, J. P.; Benoit, D.; Roy, F. *IEEE Int. Reliab. Phys. Symp. Proc.* **2014**, 1–6.

(13) Shockley, W.; Read, W. T. *Phys. Rev.* **1952**, *87* (5), 835–842.

(14) Sinton, R. A.; Cuevas, A. *Appl. Phys. Lett.* **1996**, *69* (17), 2510–2512.

(15) Castagné, R.; Vapaille, A. *Surf. Sci.* **1971**, *28* (1), 157–193.

(16) Tjzrman, L. M.; Yorktown Heights, I. B. M.; York, N. *Solid State Electron.* **1962**, *5*, 285–299

(17) Engel-Herbert, R.; Hwang, Y.; Stemmer, S. *J. Appl. Phys.* **2010**, *108* (12).

(18) Goetzberger, E. H. N. A. *bell Syst. Tech. J.* **1967**, *XLVI*

(19) Wilson, M. **2003**, *220* (March 2001), 220–225.

(20) Fernández Garrillo, P. A.; Grévin, B.; Chevalier, N.; Borowik, L. *Rev. Sci. Instrum.* **2018**, *89* (4).

(21) Hoppe, H.; Glatzel, T.; Niggemann, M.; Hinsch, A.; Lux-Steiner, M. C.; Sariciftci, N. S. *Nano Lett.* **2005**, *5* (2), 269–274.

(22) Fernández Garrillo, P. A.; Borowik, Ł.; Caffy, F.; Demadrille, R.; Grévin, B. *ACS Appl. Mater. Interfaces* **2016**, *8* (45), 31460–31468.

(23) Tennyson, E. M.; Garrett, J. L.; Frantz, J. A.; Myers, J. D.; Bekele, R. Y.; Sanghera, J. S.; Munday, J. N.; Leite, M. S. *Adv. Energy Mater.* **2015**, *5* (23), 1–8.

(24) Borowik; Lepage, H.; Chevalier, N.; Mariolle, D.; Renault, O. *Nanotechnology* **2014**, *25* (26).

(25) Sugawara, Y.; Kou, L.; Ma, Z.; Kamijo, T.; Naitoh, Y.; Jun Li, Y. *Appl. Phys. Lett.* **2012**, *100* (22).

(26) Ma, Z. M.; Kou, L.; Naitoh, Y.; Li, Y. J.; Sugawara, Y. *Nanotechnology* **2013**, *24* (22).

(27) Garrett, J. L.; Munday, J. N. *Nanotechnology* **2016**, *27* (24).

(28) Kronik, L.; Shapira, Y. *Surf. Interface Anal.* **2001**, *31* (10), 954–965.

(29) D.K.Schroder. *IEEE Trans. Electron Devices* **1997**, *44* (1), 160–170

(30) Kronik, L.; Shapira, Y. *Surf. Sci. Rep.* **1999**, *37* (1), 1–206.

(31) Hamers, R. J.; Markert, K. *Phys. Rev. Lett.* **1990**, *64* (9), 1051–1054.

(32) Dingemans, G.; Terlinden, N. M.; Pierreux, D.; Profijt, H. B.; Van De Sanden, M. C. M.; Kessels, W. M. M. *Electrochem. Solid-State Lett.* **2011**, *14* (1), 2–5.